Engineering Journal issn: 0125-8281

Article

Thermomechanical Performance of the Offset Crankshaft Heat Engine Driven by TiNiCu Shape Memory Alloys

Kasama Srirussamee[1], Anak Khantachawana[2,3], Bunheng Hok[4], and Aphinan Phukaoluan[5,*]

1 Department of Biomedical Engineering, School of Engineering, King Mongkut's Institute of Technology Ladkrabang, Bangkok 10520, Thailand
2 Department of Mechanical Engineering, Faculty of Engineering, King Mongkut's University of Technology Thonburi, Bangkok 10140, Thailand
3 Biological Engineering Program, Faculty of Engineering, King Mongkut's University of Technology Thonburi, Bangkok 10140, Thailand
4 Department of Energy Engineering, Faculty of Engineering and Technology, Siam Technology College, Bangkok 10600, Thailand
5 Energy and Environmental Management Program, Faculty of Engineering and Technology, Siam Technology College, Bangkok 10600, Thailand
*E-mail: aphinanp@siamtechno.ac.th (Corresponding author)

Abstract. Geothermal hot springs are among the alternative clean energy sources to the fossil fuels for mitigating the current global warming crisis. However, the accessible geothermal water at the surface was mostly at low temperature, which impairs the practicality of harvesting these energy. Shape memory alloys (SMAs), which deform through the increased temperature, were adapted into the rotating mechanism as the actuators with the aims to convert the low-temperature heat into the mechanical work. This study utilized the helical spring-shaped TiNiCu SMAs as the actuators for the offset crankshaft heat engine. Performance of this engine was evaluated using rope brake dynamometer, by which the rotational speed, torque, and power were measured at the water temperature from 55-85°C. The results show that the engine performance increased with increasing water temperature and was dependent on the crankshaft arrangement. The offset angle of 30° was found to be optimal in this study with maximum torque of more than 5.8 N·m and maximum power of 3.9 W at 15.7 rpm when operating at water temperature of 85°C. This study shows that the heat engine driven by TiNiCu SMAs could harvest low-temperature energy from the geothermal hot springs with the maximum observable efficiency of around 1.4%.

Keywords: Geothermal energy, shape memory alloys, heat engine

ENGINEERING JOURNAL Volume 25 Issue 2
Received 24 July 2020
Accepted 29 December 2020
Published 28 February 2021
Online at https://engj.org/
DOI:10.4186/ej.2021.25.1.85

1. Introduction

Global warming is currently considered as one of the most concerning issues for the world's population [1]. It is reportedly responsible for the rise in the average temperature of the earth's surface, which could be as high as 6°C increase by the end of the 21st century [1]. Emission of the greenhouse gases is the major cause of this phenomenon, of which the majority of them are produced by the internal combustion engines [2, 3]. Several approaches are implemented in order to mitigate this cause, such as the use of hydrogen or solar energy [4-6]. Furthermore, geothermal energy are also one of the potential clean energy source alternatively to the fossil fuels, which could be in the form of hot spring [7]. Despite its high availability, the obstacle for harvesting the energy from these geothermal sources is the massive heat loss and, consequently, the temperature of accessible geothermal water on the surface is mostly lower than the boiling point [7-9]. More often than not, these types of energy source are still regarded as the "low grade" energy [9-11]. Hence, it is impractical to convert them into the mechanical work without drilling from tens to thousands of meters below the surface as seen in the geothermal heat pump system [12, 13].

During the past decades, there were attempts to design an alternative heat engine using shape memory alloys (SMAs) [9, 10, 14, 15]. The common type of these alloys is composed of titanium and nickel (TiNi) at around 50 atomic percent each [16, 17]. Generally, there are two crystallographic phases within the SMA structure: martensite; and austenite. Martensite, which is B19' monoclinic, is stable at low temperature and freely deformable. Austenite, on the other hand, is B2 cubic and is stable at higher temperature than martensitic phase [16-18]. Furthermore, this phase is also called the "parent phase" as it is the phase that memorizes the alloy's original shape. Once the alloys are deformed at their martensitic phase and subsequently heated into the austenitic phase, the alloys would recover their original shape [9, 16, 18]. From the engineering point of view, this mechanism converts heat into the mechanical work through the structural deformation, and *vice versa* [9, 10, 14]. Moreover, the structural transformation of SMAs typically occurs at the temperature range close to those found in the accessible geothermal water, and thus it is possible to use the alloys as the heat engine actuators to harvest the geothermal energy [8-10, 17]. In addition, copper (Cu) was further added into the TiNi SMAs to improve their cyclic deformation and structural transformation stabilities, as well as increasing their thermal efficiency [19, 20]. Besides, the presence of Cu also reduces the austenitic transformation of the TiNi-based SMAs, which makes TiNiCu SMAs more compatible with low-temperature heat source than TiNi alone due to the lower operating temperature and transformation hysteresis [21, 22].

The mechanism of the SMA-driven heat engines is based on the asymmetric deformation of the alloy at one side of the engine, where the temperature exceeds the austenitic transformation [23]. This deformation perturbs the system stability and consequently triggers the engine movement. Furthermore, the heated part of the alloy is subsequently cooled down whilst travelling past the other side of the engine, where the temperature is below the martensitic transformation [23]. Hence, the engine is driven continuously, as long as the temperature of the system remains unchanged. The previous designs of the movement mechanism for the SMA-driven heat engines have come across twin crankshaft, offset crankshaft, simple pulley, reciprocating, tilted discs, and turbine [11, 23]. The power output of these designs were reported to be ranging from 0.23 to 665 W [23]. Moreover, it was also suggested that the offset crankshaft engine provides more balanced performance between the output power, motion smoothness, and fluid resistance than simple pulley and twin crank engines [24]. On the other hand, to the authors' knowledge, it has not yet been investigated how well the TiNiCu SMAs could perform when used as the offset crankshaft heat engine actuators. Hence, it is of interest to this study to assemble the offset crankshaft heat engine and pursue two novel proof-of-concept objectives: to evaluate the performance of TiNiCu-driven offset crank heat engine; and to optimize the offset angle of heat engine for low-temperature heat source. Thermomechanical performance of the assembled heat engine at the offset angle of 0°, 10°, 20°, 30°, and 40° were evaluated and presented in this paper, including the rotational speed, torque, and the thermal efficiency, at water temperature ranging from 55°C to 85°C with 5°C increment.

2. Materials and Methods

2.1. TiNiCu Shape Memory Alloys (SMAs)

TiNiCu wires with the diameter of 0.7 mm (NT-H8 As-Drawn, Furukawa Techno Material) were used in this study. The wires were shaped into the helical spring-like structure with the inner spring diameter of 4 mm (spring index of 6.71) and 60 mm in length. The shaped wires were annealed at 350°C for 30 min with the argon flow (Linde Thailand) at 5 L/min as optimized in our previous study [25]. The wires were quenched in ice-cold water immediately after the annealing process. Finally, the surface of the wires was cleaned by 1-min etching with the mixture of 48% hydrofluoric acid (LobaChemie), 70% nitric acid (UNIVAR®, Ajax Finechem), and distilled water at the volume ratio of 1:4:5, respectively. The phase transformation temperatures of TiNiCu SMAs used in this study have already been characterized and presented in our previous report, of which the data are shown in Table 1 [25].

Table 1. The austenitic and martensitic transformation temperatures of the TiNiCu SMAs used in this study.

Heating (Austenite)		Cooling (Martensite)		Ref.
Start	Finish	Start	Finish	
32.9°C	60.2°C	48.0°C	15.8°C	[25]

2.2. Offset Crankshaft SMA Heat Engine Design

The schematics of the offset crankshaft heat engine assembled in this study are shown in Fig. 1(a, b). The engine was composed of two eccentric rotating wheels, of which the outer wheel was 500 mm in diameter and that of the inner wheel was 120 mm. The length of the outer and inner wheels were 500 mm and 320 mm, respectively. There were 9 rows of TiNiCu SMA actuators connecting between two wheels, and each row contains 16 actuators with 19 mm apart. The distance between rows along the outer and inner wheel circumferences were 147.5 mm and 39.5 mm, respectively. The working displacement of each actuator was 100 mm, based on the difference between maximum and minimum distance between the surface of the outer and inner wheels. This degree of spring displacement corresponds to the material shear strain of 0.012 [26]. The off-center distance was set at 50 mm with adjustable offset angle.

Following the assembly, the heat engine was installed into the steel-framed acrylic water tank with 50 x 95 x 24 cm3 in size (width x length x depth), in which the rotating axis of the engine was located at the center of the length and in parallel to the width of the tank. The water was filled in the tank until it reached the lower surface of the inner wheel and subsequently heated by four 3-kW heating coils (Thermo+, Vaicharoen Heater) located at each corner of the tank. Two 11-cm cooling fans (12-V Brushless DC San Ace, SANYO DENKI) were also installed at each side of the engine to enhance the cooling through forced convection, Fig. 1(c). The corresponding air speed was approximately 6.3 m/s measured by digital anemometer (GM816, BENETECH). Moreover, this study has also modified the arrangement of the actuators into the thread-like manner in order to increase the contact between the cooling air and the actuator surface as shown in Fig. 1(d).

2.3. Rope Brake Dynamometer

In order to evaluate the thermomechanical performance of the assembled heat engine, the in-house made rope brake dynamometer with 0.18-m pulley and variable dead weight between 0 and 7.6 kgf was attached to the rotating shaft as presented in Fig. 2(a, b) [27].

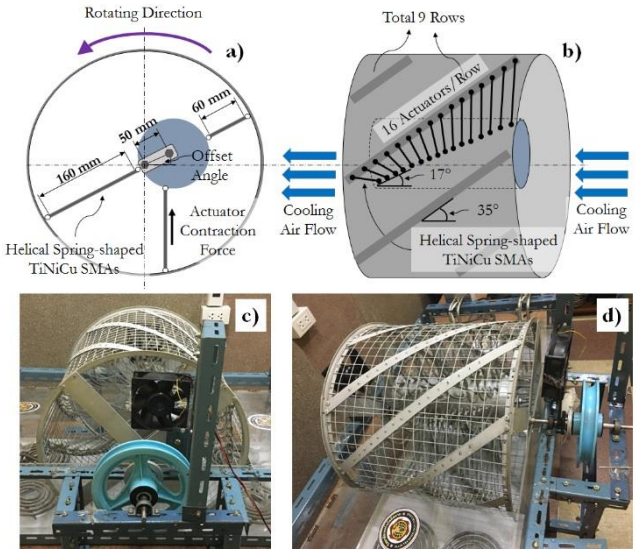

Fig. 1. The front-view (a) and side-view (b) illustrations and the corresponding actual images (c, d) of the assembled offset crankshaft SMA heat engine in this study.

Forces at the offset angle between 0° and 40° were measured using digital weighing scale (WH-A04, WeiHeng) during the operation at the nominal water temperature between 55°C and 85°C, using which torque exhibited by the engine at each experimental condition could be calculated using Eq. (1). On the other hand, digital timer and manual revolution counter were used to determine the average corresponding rotational speed in order to calculate the mechanical output power of the engine using Eq. (2). Moreover, digital thermocouples with the accuracy of ±1°C were also used to detect the actual water temperature and cooling temperature at each nominal water temperature, of which the latter was measured from the cooling air after flowing past the actuators. The average actual temperatures during the rope brake dynamometer test are shown in Table 2.

$$T = (W_t - W_s) \times g \times \frac{D_w}{2} \quad (1)$$

where T = Torque (N·m)

W_t = Dead weight (kgf)

W_s = Readable force from the digital scale (kgf)

g = Gravitational acceleration (9.81 m/s²)

D_w = Diameter of dynamometer (0.18 m)

$$P_{out} = T\frac{2\pi N}{60} \quad (2)$$

where P_{out} = Mechanical output power (W)

T = Torque (N·m)

N = Heat engine rotational speed (rpm)

DOI:10.4186/ej.2021.25.2.85

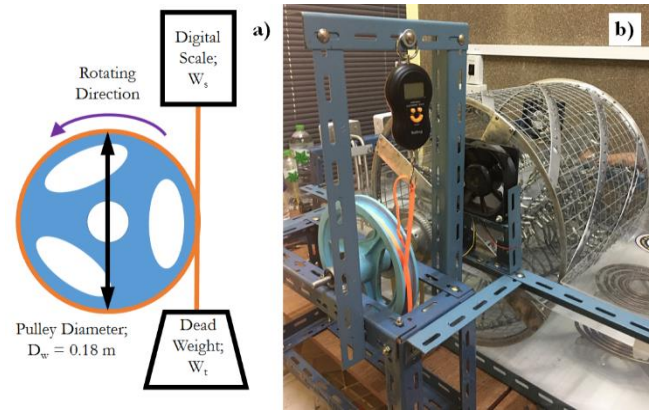

Fig. 2. The schematic (a) and actual image (b) of the rope brake dynamometer setup in this study.

Table 2. Actual heating and cooling temperatures during the rope brake test.

Nominal Water Temp.	Average Actual Water Temp.	Average Cooling Temp.
55°C	55.5°C	37.1°C
60°C	60.4°C	37.8°C
65°C	65.3°C	39.6°C
70°C	70.3°C	41.3°C
75°C	75.2°C	43.2°C
80°C	80.3°C	45.1°C
85°C	85.4°C	46.0°C

2.4. Thermomechanical Efficiency Evaluation

Thermomechanical efficiency of the assembled heat engine was calculated by dividing the exhibited mechanical work (W_{out}) with heat required for austenitic transformation of the SMAs (Q_{in}). On one hand, the exhibited mechanical work per revolution was calculated from the mechanical power divided by the rotational speed. On the other hand, heat per unit mass required for one cycle of austenitic transformation was analyzed from the endothermic peak area of the DSC data from our previous study [25] as shown in Fig. 3 [28] using ImageJ 1.52a software [29]. The obtained heat per unit mass was multiplied by total mass of the actuators (2.51 g x 144 actuators) in order to obtain Q_{in} per revolution, assuming that all the springs underwent austenitic transformation homogenously from martensitic phase in every revolution. The Q_{in} at each water temperature are shown in Table 3.

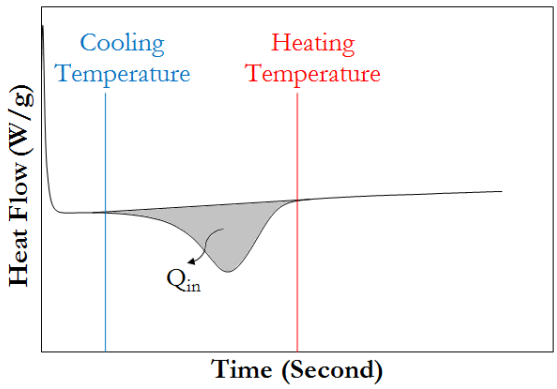

Fig. 3. The quantification of heat required for austenitic transformation (Qin) of the TiNiCu shape memory alloys used in this study.

Table 3. The value of Q_{in} at each nominal water temperature obtained from the endothermic peak of the DSC data.

Nominal Water Temp.	Q_{in} (J)
55°C	3,362
60°C	3,763
65°C	3,633
70°C	3,425
75°C	3,105
80°C	2,742
85°C	2,553

3. Results

3.1. Thermomechanical Performance of the Assembled Heat Engine: Torque; Power; and Efficiency

Figures 4(a-e) show the results from rope brake dynamometer, which present the inverse relationship between torque and the corresponding rotational speed measured from the assembled heat engine at various water temperature. It was found that, by increasing water temperature, the rotational speed at each level of torque was increased. Maximum rotational speed was achieved when there was no load, i.e. zero torque, and *vice versa*. Moreover, changes in the engine offset angle could also influence the torque exhibited, in which the maximum trend of torque and rotational speed was found in the offset angle of 30°C at 85°C water temperature with more than 5.8 N·m and 33 rpm, respectively.

Furthermore, the mechanical power of the assembled heat engine at each condition are shown in Fig. 5(a-e), which were the multiplication between torque and the corresponding rotational speed. The results present bell-shaped relationship between mechanical power and the corresponding rotational speed, since there was no power at either zero torque, or zero rotational speed. Similarly to torque, maximum power was increased with increasing water temperature and was at maximum at the

offset angle of 30°C with 3.9 W and the corresponding torque of 2.3 N·m, based on the peak of the fitted function at 85°C water temperature as shown in Fig. 6. On the other hand, it was also noticeable that the maximum power increased steadily with increasing water temperature, whereas there was no significant increase in torque at maximum power at the water temperature above 75°C.

In terms of the thermomechanical efficiency, it was shown in Fig. 7(a-e) that the relationship between the efficiency and rotational speed was inverse. In other words, the thermomechanical efficiency tended to be higher at lower rotational speed. The maximum observable efficiency was around 1.4% when operating at water temperature of 85°C, regardless of the offset angle. However, when operating at maximum power, it appears that the thermomechanical efficiency also increased with increasing water temperature as shown in Fig. 8. The maximum efficiency at maximum power between 0.50% and 0.56% were observed at the water temperature between 80°C and 85°C in all the offset angles, except for 0°, where the efficiency at maximum power was only the highest at water temperature of 85°C.

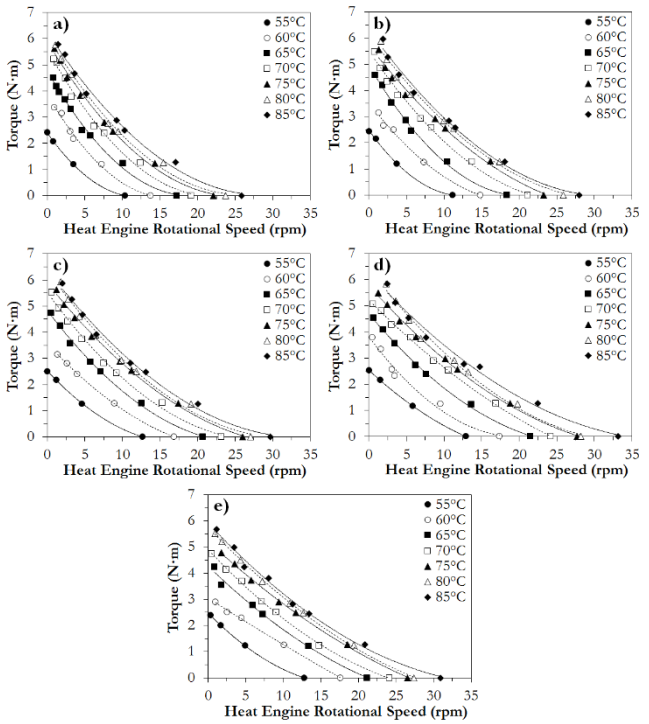

Fig. 4. Torque exhibited by the assembled heat engine at different offset angles: a) = 0°; b) = 10°; c) = 20°; d) 30°; and e) 40°, when operating at water temperature ranging from 55°C to 85°C. The fitted trend lines were 2nd order polynomial.

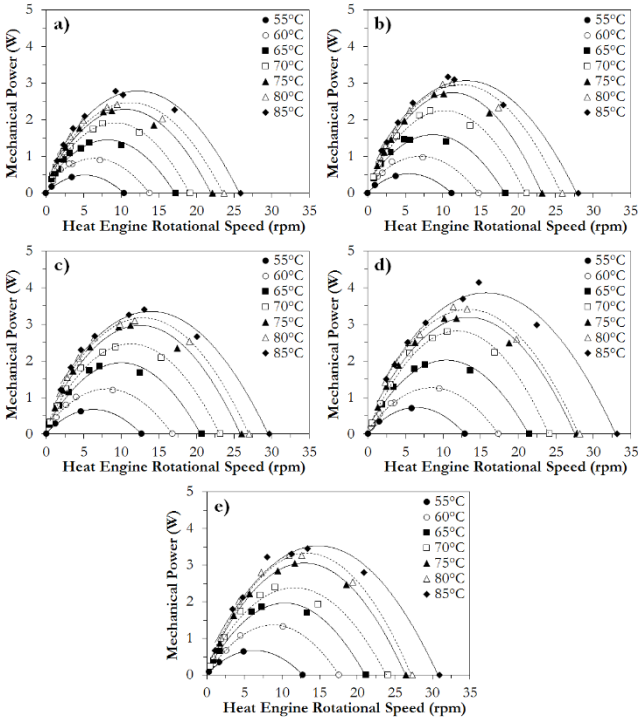

Fig. 5. Mechanical power exhibited by the assembled heat engine at different offset angles: a) = 0°; b) = 10°; c) = 20°; d) 30°; and e) 40°, when operating at water temperature ranging from 55°C to 85°C. The fitted trend lines were 2nd order polynomial.

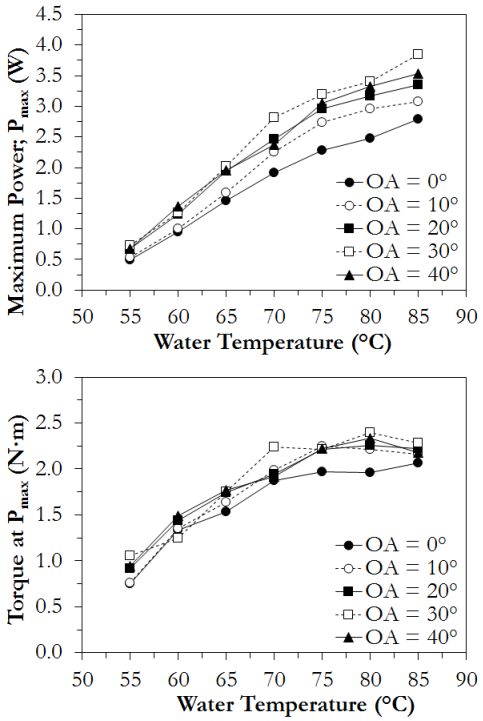

Fig. 6. Empirically fitted maximum mechanical power (left) and the corresponding torque (right) exhibited by the assembled heat engine at different offset angles (OA), when operating at water temperature ranging from 55°C to 85°C.

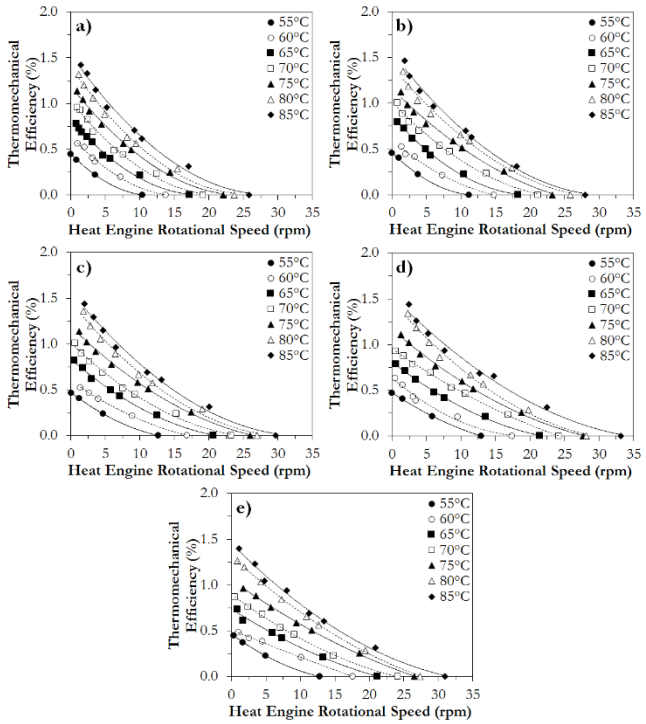

Fig. 7. Thermomechanical efficiency of the assembled heat engine at different offset angles: a) = 0°; b) = 10°; c) = 20°; d) 30°; and e) 40°, when operating at water temperature ranging from 55°C to 85°C. The fitted trend lines were 2nd order polynomial.

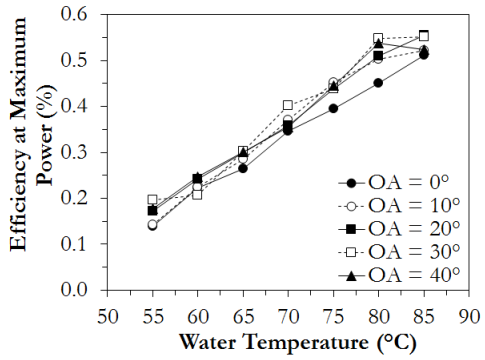

Fig. 8. Corresponding thermomechanical efficiency at the maximum mechanical power exhibited by the assembled heat engine at different offset angles (OA), when operating at water temperature ranging from 55°C to 85°C.

4. Discussion

The results from this study demonstrate that TiNiCu SMAs were capable of driving the offset crankshaft mechanism upon the exposure to the hot water at above their austenitic transformation temperature, which converted heat into the useable mechanical work. Moreover, the performance of the assembled heat engine was also found to be dependent on both the water temperature and the crankshaft arrangement, i.e. the offset angle. These proof-of-concept findings are discussed further in details in the following sections.

4.1. Working Temperature of TiNiCu SMAs as the Actuators

According to the concept of DSC, the endothermic peak from the DSC indicates the heat consumed by the alloys during structural transformation towards the austenitic phase, whereas the exothermic peak was the heat released from the alloys as a result of martensitic transformation [28]. Hence, the beginning and ending of each peak were the temperature at which phase transformation is started and completed, respectively. It has been reported that the presence of Cu within the TiNi structure at 7.5 atomic percent could reduce the austenitic finish temperature of the SMAs down to 25°C [30]. On the other hand, the austenitic transformation of the TiNiCu observed in this study was finished at around 60.2°C, which is in the range suggested by the manufacturer [25]. However, the actual Cu content of the SMAs used in this study was proprietary. Furthermore, it should be noted that the austenite finish temperature are also dependent on the material processing methods, e.g. annealing and cold working conditions, in addition to the Ti, Ni, and Cu contents [21, 31, 32]. It is also worth pointing out that the transformation temperature of TiNiCu SMAs obtained by DSC also depends on the heating and cooling rate, though it was not reported whether the endothermic heat was also affected [30]. On the contrary, it appears that the influence of DSC heating and cooling rate on the transformation temperature and endothermic heat of TiNi SMAs was less significant [33].

It is understood that this TiNiCu alloys could perform best as an actuator within the heating temperature of 60.2°C or higher and cooling temperature of 15.8°C and lower. However, during the study, it was impractical to achieve the constant cooling temperature below room temperature without dedicated cooling system and control. Since the cooling fans were used in this proof-of-concept study, the average actual cooling temperature was varied between 37.1 and 46.0°C, depending on the hot water temperature underneath the engine.

4.2. Effect of Water Temperature on the Heat Engine Performance

The results from this study show that the maximum rotational speed, torque, and mechanical power increased with increasing temperature. This is potentially due to the higher heating rate provided for the austenitic transformation of the alloys. The higher water temperature, the faster the alloys reach their austenite phase and thus generate the driving force for the heat engine. Moreover, an increase in water temperature also enhanced the thermomechanical efficiency. It is our thought that this is due to the fact that both torque and rotational speed were increased at higher water temperature, and thus the mechanical power output was enhanced. Furthermore, it is also worth noting that the cooling method also plays a role in the

thermomechanical performance, since it dictates the martensitic transformation of the SMAs prior to the following heating cycle. It could be expected that once the rotational speed is increased, the cooling time is reduced, which could impair the mechanical performance once the martensitic transformation is not completed. However, the reduction in performance due to the increased water temperature was not seen in this study, potentially because of the use of cooling fans and the thread-like actuator arrangement to enhance the cooling through forced convection.

4.3. Effect of the Crankshaft Offset Angle

It was found that the crankshaft offset angle could also influence the heat engine performance in terms of rotational speed, torque, and mechanical power. The results show that the optimal offset angle was 30°, since the highest maximum power and the corresponding torque were observed. Although the exact underlying reason was still unclear, it is our thought that the alteration of the offset angle has affected the position where the SMAs were first exposed to the hot water as shown in Fig. 9. If the wires were exposed to the hot water after they reached the maximum spring displacement, there will be power loss due to the tolerance from over-extension. On the other hand, if the wires were exposed to the hot water before they reached the maximum spring displacement position, there will be loss due to the austenitic resistance. Therefore, it is expected that at 30° offset angle, the first point of contact between the wires and hot water was closest to the maximum spring displacement position than the other offset angles, which resulted in the optimal performance exhibited by the heat engine. It is believed that this finding is useful for the future design and development of the offset crankshaft heat engine driven by SMAs.

Despite a number of previous studies on the SMA heat engine, it is not practical to directly compare the performance between studies as there were differences in the actuator geometry and quantity, as well as the difference in heating and cooling methods. As a result, the reported mechanical power of the offset crankshaft heat engines could vary from 0.23 to 20 W, despite similar moving mechanism [23]. Hence, it would need some form of standardization or normalization before comparing the heat engine performance across the studies. In terms of the thermomechanical efficiency, it was once mentioned that the efficiency of the previous studies were either less than 2%, or even not reported, although the theoretical value could be as high as 9% to 25% [11, 34]. However, this is consistent with the maximum efficiency of around 1.4% observed in this study. In addition, this level of thermomechanical efficiency is also comparable to the thermoelectrical efficiency of the SMA-driven heat engine reported in the recent literature, although the working mechanism and application are different from this study [8, 35]. It can be seen that the improvement of both thermomechanical and thermoelectrical efficiencies are still being a challenge for the current and future design of the SMA-driven heat engines.

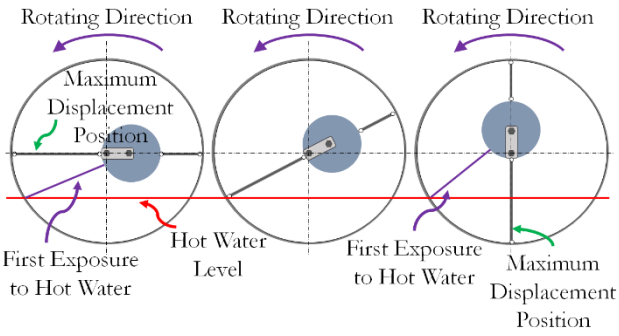

Fig. 9. The front-view illustration of the over-extension loss (left), the optimal position (center), and the austenitic resistance loss (right), during the operation of the offset crankshaft heat engine at different offset angle.

4.4. Potential Applications and Future Studies

It is shown in this study that the TiNiCu-driven heat engine could be used for converting the low-temperature geothermal energy into the useable mechanical work. Moreover, electrical generator can also be connected to the rotating shaft of this engine in order to convert the mechanical work further into the electrical energy [8]. It is plausible that the maximum performance of this heat engine design is yet to be achieved as there are opportunities to pursue further study in terms of the working displacement and number of the actuator. Furthermore, it is also worth investigating the fatigue behavior of the TiNiCu SMAs as it is likely that the heat engine performance could increase with increasing the alloy displacement that generates stronger driving force, but the life cycle of the alloys is compromised [36, 37]. On the other hand, it could still be asked whether or not the use of SMA heat engine is cost-effective, since the thermomechanical efficiency was just less than 2%. This point could be mitigated by the fact that the cost of the geothermal energy from the hot spring is low, if not zero, and the economy of scale once the engine is produced in large quantity in future [34]. Hence, it is believed by us that this proof-of-concept study would be beneficial for the future investigation on the use of engineering approaches for harvesting the alternative energy.

5. Conclusion

TiNiCu SMAs are suitable to be used as the actuators for the offset crankshaft heat engine to harvest the geothermal energy. The thermomechanical performance of the assembled heat engine was dependent on both water temperature and the crankshaft offset angle. The optimal thermomechanical performance in this proof-of-concept study was achieved

at the water temperature of 85°C and 30° crankshaft offset angle with the maximum torque of more than 5.8 N·m and maximum power of 3.9 W at 15.7 rpm. The maximum observable thermomechanical efficiency at 85°C was around 1.4%, regardless of the offset angle. Moreover, the assembled heat engine in this study can be further optimized in terms of the number and working displacement of the actuators, the fluid resistance reduction, as well as the fatigue analysis.

Acknowledgement

This work was financially supported by Siam Technology College (STC) (STC 611/2562). The authors also would like to thank Mr Vannet Yorn and Ms Saravy Dum for their assistance throughout the study.

References

[1] R. S. Ahima, "Global warming threatens human thermoregulation and survival," *The Journal of Clinical Investigation,* vol. 130, no. 2, pp. 559-561, 2020.

[2] V. Ganesan, "A comprehensive review on oxygenated fuel additive options for unregulated emission reduction from diesel engines," in *Alternative Fuels and Their Utilization Strategies in Internal Combustion Engines*, A. P. Singh, Y. C. Sharma, N. N. Mustafi, and A. K. Agarwal, Eds. Singapore: Springer Singapore, 2020, pp. 141-165.

[3] M. O. Dioha, "Modelling the impact of Nigeria household energy policies on energy consumption and CO_2," *Engineering Journal*, vol. 22, no. 6, pp. 1-19, 2018.

[4] C. Acar and I. Dincer, "The potential role of hydrogen as a sustainable transportation fuel to combat global warming," *International Journal of Hydrogen Energy,* vol. 45, no. 5, pp. 3396-3406, 2020.

[5] M. H. Mobarak, R. N. Kleiman, and J. Bauman, "Solar-charged electric vehicles: A comprehensive analysis of grid, driver, and environmental benefits," *IEEE Transactions on Transportation Electrification*, 2020.

[6] K. Kumar.N and V. Subramaniam, "Real time clock based energy efficient automatic dual axis solar tracking system," *Engineering Journal*, vol. 22, no. 1, pp. 15-26, 2018.

[7] C. Haselwimmer, A. Prakash, and G. Holdmann, "Quantifying the heat flux and outflow rate of hot springs using airborne thermal imagery: Case study from Pilgrim Hot Springs, Alaska," *Remote Sensing of Environment,* vol. 136, pp. 37-46, 2013.

[8] P. Kumar *et al.*, "Shape memory alloy engine for high efficiency low-temperature gradient thermal to electrical conversion," *Applied Energy,* vol. 251, p. 113277, 2019.

[9] M. Langan and K. O'Toole, "A new technology for cost effective low grade waste heat recovery," *Energy Procedia,* vol. 123, pp. 188-195, 2017.

[10] A. L. Browne *et al.*, "SMA heat engines: Advancing from a scientific curiosity to a practical reality," in *International Workshop: Smart Materials, Structures & NDT in Aerospace*, Montreal, Canada, 2011.

[11] R. A. Kishore and S. Priya, "A review on low-grade thermal energy harvesting: Materials, methods and devices," *Materials,* vol. 11, no. 8, p. 1433, 2018.

[12] J. Vidal and A. Genter, "Overview of naturally permeable fractured reservoirs in the central and southern Upper Rhine Graben: Insights from geothermal wells," *Geothermics,* vol. 74, pp. 57-73, 2018.

[13] J. Luo, W. Xue, T. Hu, W. Xiang, and J. Rohn, "Thermo-economic analysis of borehole heat exchangers (BHE) grouted using drilling cuttings in a dolomite area," *Applied Thermal Engineering,* vol. 150, pp. 305-315, 2019.

[14] S. M. Lahamge, S. P. Nikam, M. R. Bhingare, A. S. Bachhav, and K. R. Kumbharde, "Study and design of nitinol engine," *International Research Journal of Engineering and Technology,* vol. 5, no. 9, pp. 1500-1503, 2018.

[15] Y. Sato, N. Yoshida, Y. Tanabe, H. Fujita, and N. Ooiwa, "Characteristics of a new power generation system with application of a shape memory alloy engine," *Electrical Engineering in Japan,* vol. 165, no. 3, pp. 8-15, 2008.

[16] S. Miyazaki and H. Y. Kim, "TiNi-base and Ti-base shape memory alloys," *Materials Science Forum,* vol. 561-565, pp. 5-21, 2007.

[17] K. Otsuka and X. Ren, "Physical metallurgy of Ti–Ni-based shape memory alloys," *Progress in Materials Science,* vol. 50, no. 5, pp. 511-678, 2005.

[18] J. Mohd Jani, M. Leary, A. Subic, and M. A. Gibson, "A review of shape memory alloy research, applications and opportunities," *Materials & Design (1980-2015),* vol. 56, pp. 1078-1113, 2014.

[19] F. J. Gil and J. A. Planell, "Thermal efficiencies of NiTiCu shape memory alloys," *Thermochimica Acta,* vol. 327, no. 1, pp. 151-154, 1999.

[20] F. J. Gil and J. A. Planell, "Effect of copper addition on the superelastic behavior of Ni-Ti shape memory alloys for orthodontic applications," *Journal of Biomedical Materials Research,* vol. 48, no. 5, pp. 682-688, 1999.

[21] S. Dilibal, H. Adanir, N. Cansever, and A. F. Saleeb, "Comparison and characterization of NiTi and NiTiCu shape memory alloys," in *Proceedings of the 6th IAASS Conference - Safety is Not an Option*, Montreal, Canada, 2013.

[22] T. H. Nam, T. Saburi, and K. i. Shimizu, "Cu-content dependence of shape memory characteristics in Ti-Ni-Cu alloys," *Materials Transactions, JIM,* vol. 31, no. 11, pp. 959-967, 1990.

[23] H. Tobushi, K. Date, and K. Miyamoto, "Characteristics and development of shape-memory alloy heat engine," *Journal of Solid Mechanics and Materials Engineering,* vol. 4, no. 7, pp. 1094-1102, 2010.

[24] H. Tobushi, K. Kimura, H. Iwanaga, and J. R. Cahoon, "Basic research on shape memory alloy heat engine: Output power characteristics and problems in development," *JSME International Journal. Ser. 1, Solid Mechanics, Strength of Materials,* vol. 33, no. 2, pp. 263-268, 1990.

[25] C. Thanarwathnarrong, A. Khantachawana, and A. Phukaoluan, "Influence of heat treatment temperature on recovery force spring used for actuator of heat engine," *Journal of Energy and Environment Technology,* vol. 6, no. 2, pp. 39-46, 2019.

[26] J. Ma, H. Huang, and J. Huang, "Characteristics analysis and testing of SMA spring actuator," *Advances in Materials Science and Engineering,* vol. 2013, p. 823594, 2013.

[27] J. S. Killedar, "Dynamometer - Classification and types," in *Dynamometer: Theory and Application to Engine Testing*: Xlibris US, 2012, pp. 41-67.

[28] J. A. Shaw, C. B. Churchill, and M. A. Iadicola, "Tips and tricks for characterizing shape memory alloy wire: Part 1—Differential scanning calorimetry and basic phenomena," *Experimental Techniques,* vol. 32, no. 5, pp. 55-62, 2008.

[29] W. S. Rasband, "ImageJ (1.52a)," U.S. National Institutes of Health, Bethesda, Maryland, USA, 2018.

[30] Z. G. Wang, X. T. Zu, and Y. Huo, "Effect of heating/cooling rate on the transformation temperatures in TiNiCu shape memory alloys," *Thermochimica Acta,* vol. 436, no. 1, pp. 153-155, 2005.

[31] H. Du and Y. Fu, "Deposition and characterization of Ti1−x(Ni,Cu)x shape memory alloy thin films," *Surface and Coatings Technology,* vol. 176, no. 2, pp. 182-187, 2004.

[32] A. Phukaoluan, A. Khantachawana, P. Kaewtatip, S. Dechkunakorn, and J. Kajornchaiyakul, "Improvement of mechanical and biological properties of TiNi alloys by addition of Cu and Co to orthodontic archwires," *International Orthodontics,* vol. 14, no. 3, pp. 295-310, 2016.

[33] C. G. Slough, "A study of the nitinol solid-solid transition by DSC," TA Instruments, New Castle, DE, USA, 2007.

[34] E. H. Schiller, "Heat engine driven by shape memory alloys: Prototyping and design," Master of Science in Mechanical Engineering, Virginia Polytechnic Institute and State University, 2002.

[35] A. Dragan, A. K. Ravi, V. Dushan, and P. Shashank, "Miniature shape memory alloy heat engine for powering wireless sensor nodes," *Energy Harvesting and Systems,* vol. 1, no. 1-2, pp. 13-18, 2014.

[36] G. S. Mammano and E. Dragoni, "Functional fatigue of shape memory wires under constant-stress and constant-strain loading conditions," *Procedia Engineering,* vol. 10, pp. 3692-3707, 2011.

[37] C. A. Calhoun, "Actuation fatigue of shape memory alloys," Master of Science, Texas A&M University, 2012.

Kasama Srirussamee, photograph and biography not available at the time of publication.

Anak Khantachawana, photograph and biography not available at the time of publication.

Bunheng Hok, photograph and biography not available at the time of publication.

Aphinan Phukaoluan, photograph and biography not available at the time of publication.